ChemComm

COMMUNICATION

View Article Online
View Journal

Cite this: DOI: 10.1039/d5cc03175c

Received 5th June 2025,
Accepted 19th June 2025

DOI: 10.1039/d5cc03175c

rsc.li/chemcomm

Structure–property relationships in disodium anthracene dicarboxylate for sodium-ion storage *via* 3D electron diffraction†

Aamod V. Desai, [ab] Heitor S. Seleghini, [ac] Daniel N. Rainer, [d] Maximillian G. Stanzione, [a] David B. Cordes, [a] Oxana V. Magdysyuk, [a] Aidan P. McKay, [a] Simon J. Coles, [d] Sharon E. Ashbrook, [ac] Russell E. Morris *[abc] and A. Robert Armstrong *[ab]

Organic materials are increasingly commanding attention as a sustainable choice for charge storage in rechargeable batteries. To fully realise their promise, significantly more understanding is needed in terms of structure–property correlations. Here we report a highly conjugated molecule, disodium anthracene-9,10-carboxylate (Na_2ADC), synthesised using rapid microwave-assisted heating and evaluated as an anode material in sodium-ion batteries. Detailed material characterisation is reported, including the crystal structure determined from three-dimensional electron diffraction (3D ED) studies, demonstrating the suitability and advantage of this method for the structural characterisation of organic electrode materials. This study highlights the role of molecular design and structural properties in facilitating the delivery of high-performing organic electrode materials.

Sodium-ion batteries (SIBs), which are viewed as a drop-in technology for the widely commercialised Li-ion batteries (LIBs), are emerging as a sustainable outlet for energy storage.[1] SIBs present several advantages, including but not limited to, lower cost, greater abundance of sodium in the Earth's crust and safer operation.[2,3] Despite these benefits, the direct transition of electrode materials from LIBs to SIBs is non-trivial and requires the development of active solids suited to the purpose.[4] Research into organic electrode materials (OEMs) for use in sustainable energy storage devices has witnessed continual growth, both in anodes and cathodes.[5–8] Their rich chemistry provides a handle to tune redox activity by varying the functional group and the core of the molecule.[9,10] For anode materials in rechargeable batteries, organic materials with several functional groups such as imine, azo, and carboxylate, are suitable targets, with a low working voltage and moderate to high specific capacities.[11] Sodium carboxylates, a subset of OEMs, are promising candidates owing to their high performance and ease of synthesis with lower environmental impact.[12] The carboxylate group is understood to be the reaction centre with a reversible one-electron insertion per active site.[13] The presence of secondary functional groups or different molecular backbones affects the reaction potential, and in certain cases the cycling stability.[14–18] Small molecule OEMs, in general, are susceptible to side reactions with the electrolyte or dissolution upon cycling. Changing the molecular size, polarity or polymerisation has been suggested to improve cycle life.[19,20] Despite the progress of research into sodium carboxylates, both in terms of range of molecules and their electrochemical features, there is a need to understand the structure–property correlation in such systems, with the aim of delivering high-performing OEMs. Here, we examine a sodium carboxylate with a highly conjugated core, disodium anthracene-9,10-dicarboxylate (Na_2ADC), for charge storage in SIBs. Na_2ADC was synthesised using the greener approach[12,21] of microwave-assisted irradiation and detailed material characterisation was carried out, including the crystal structure determination from three-dimensional electron diffraction (3D ED) studies. Na_2ADC exhibited sodium-ion insertion at a low potential along with stable cycling capacities.

The title compound, Na_2ADC, was synthesised using microwave-assisted heating (hereafter referred to as Na_2ADC(MW)), using the same protocol previously optimised for preparing sodium carboxylates (Fig. 1a, experimental details in ESI†).[22] Owing to their high ionic character, materials such as sodium carboxylates can be harder to grow as large single crystals that do not contain any lattice solvent molecules. This makes traditional single-crystal X-ray diffraction challenging, but can be overcome by employing electron diffraction, which can be used for single crystallites that are considerably smaller in size. Inspired by the success of utilising electron diffraction to determine crystal structures of metal–organic frameworks (MOFs) and covalent organic frameworks

[a] EaStCHEM School of Chemistry, University of St Andrews, North Haugh, St Andrews KY16 9ST, UK. E-mail: rem1@st-andrews.ac.uk, ara@st-andrews.ac.uk
[b] The Faraday Institution, Quad One, Harwell Science and Innovation Campus, Didcot, OX11 0RA, UK
[c] St Andrews Centre of Magnetic Resonance, University of St Andrews, North Haugh, St Andrews KY16 9ST, UK
[d] School of Chemistry and Chemical Engineering, University of Southampton, University Road, Southampton, SO17 1BJ, UK

† Electronic supplementary information (ESI) available. See DOI: https://doi.org/10.1039/d5cc03175c

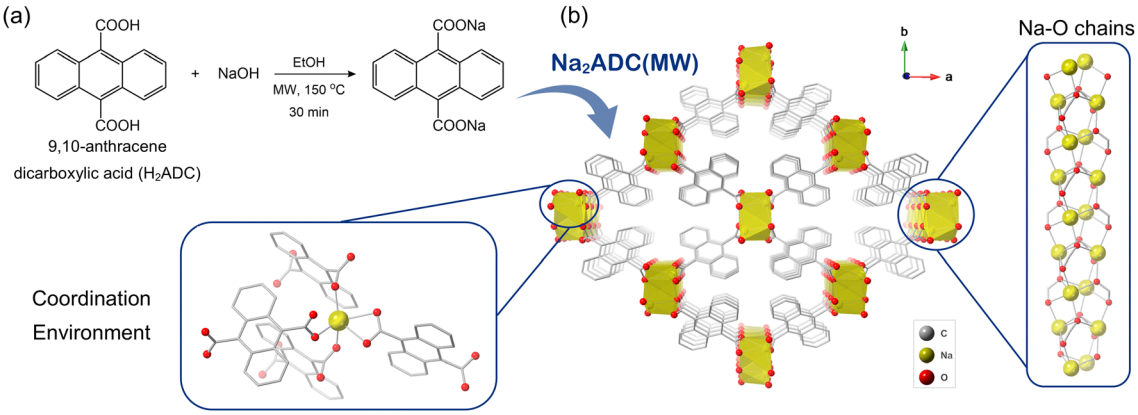

Fig. 1 (a) Reaction scheme for the preparation of Na_2ADC using microwave (MW)-assisted heating. (b) Perspective view of the structural packing diagram in Na_2ADC, with zoomed views alongside of the inorganic chain and coordination environment around the sodium ions (colour codes: C, grey; Na, yellow; O, red. H atoms are omitted for clarity).

(COFs),[23,24] the structure elucidation of Na_2ADC(MW) was completed using the 3D ED technique from powder samples (details in the experimental section). Na_2ADC(MW) adopts an orthorhombic crystal structure, space group *Pccn*, and the asymmetric unit comprises one Na cation, and half of the deprotonated linker (Fig. S1 and Table S1, ESI†). Each Na-ion is coordinated by O atoms of the carboxylate group from four independent ligands, and the overall structure consists of Na–O chains running along the crystallographic *c*-axis (Fig. 1b and Fig. S2, ESI†), with the chains linked by the anthracene moieties. The H atoms of carbon C3 of the aromatic group have a non-covalent, edge-to-face CH/π interaction[25] with the anthracene core of the neighbouring linker (Fig. S3, ESI†). These interactions cause the structural packing to be significantly different from related sodium carboxylates that feature a pillared-layer framework (Fig. S2 and S4, ESI†).[26–28] Also, in the case of Na_2ADC(MW), the steric bulk caused by the additional aromatic rings in the anthracene causes the carboxylate groups to bend much more relative to the aromatic core (Fig. S5, ESI†). This leads to the absence of Na–O sheets previously reported for similar sodium carboxylates that feature a planar geometry in the organic building unit (Fig. S6, ESI†). It is worth noting that the current result successfully demonstrates the use of 3D ED for determining the crystal structures of sodium carboxylates.

The material was further characterised *via* several techniques. The powder X-ray diffraction (PXRD) pattern showed good agreement with the calculated pattern and the absence of any peak corresponding to unreacted linker (Fig. S7, ESI†). Agreement of elemental analysis results with the expected values (details in experimental methods, ESI†), further validated the bulk phase purity. Both Fourier-transform infrared (FT-IR) and Raman spectra also confirmed the formation of the product with the absence of peaks corresponding to unreacted linker (Fig. S8 and S9, ESI†). The ^{13}C CP MAS NMR spectra of the linker and Na_2ADC(MW) (Fig. S10, ESI†) showed no unreacted carboxyl groups, *i.e.*, COOH rather than COONa, due to the presence of a single signal at a higher chemical shift (~180.3 ppm) when compared to the linker (~176.4 ppm). The ^{13}C signals were assigned using Gauge Including Projector Augmented Waves (GIPAW) DFT calculations as shown in Table S3 (ESI†). The structure of Na_2ADC(MW) obtained from 3D ED contains a single sodium environment, in good agreement with the ^{23}Na MAS and ^{23}Na MQMAS NMR spectra of the pristine material (Fig. 2), which both contain a well-defined single line shape with features characteristic of second-order quadrupolar broadening.[29] The ^{23}Na NMR parameters calculated from the crystal structure using DFT agree well with the experimental spectra (see Table S4, ESI†). The sodium atoms in the inorganic chains adopt a distorted trigonal bipyramid geometry (Fig. 1), resulting in a higher quadrupolar constant ($C_Q \approx 3.3$ MHz) compared with other sodium carboxylates with pillared-layer architectures previously reported by Whewell *et al.*[30] Scanning electron microscopy (SEM) images showed that the powder is an aggregation of small particles of <1 μm and no well-defined morphology (Fig. S12, ESI†). Thermogravimetric analysis (TGA). showed no significant mass loss below 500 °C (Fig. S13, ESI†). The thermal stability is comparable to a related molecule, Na_2NDC (disodium naphthalene-2,6-dicarboxylate), which is stable up to 500 °C.[31] The corresponding structural properties of Na_2ADC(MW) were investigated by variable temperature PXRD (VT-PXRD) under continuous argon gas flow (details in ESI†). As seen in the TGA profile, the structure remained unaltered up to 475 °C, with only subtle peak shifts

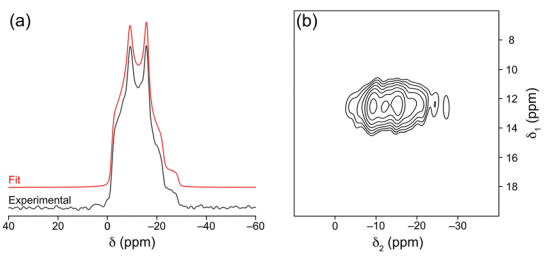

Fig. 2 (a) ^{23}Na (14.1 T, 16 kHz MAS) MAS NMR spectrum of Na_2ADC(MW) (black line) and line shape simulated using parameters determined by analytical fitting (see Table S4 in the ESI†). (b) ^{23}Na (14.1 T, 16 kHz MAS) MQMAS spectrum of Na_2ADC(MW) acquired using an amplitude-modulated *z*-filter pulse sequence and shown after shearing.

corresponding to thermal expansion (Fig. S14, ESI†). On heating, the cell parameters increase along the *b*- and *c*-axes while largely remaining unaltered along the *a*-axis (Fig. S15, ESI†). The cell volume also undergoes a gradual expansion associated with thermal expansion. In the quartz tube used for heating the sample, crystals were obtained on the cooler part of the tube (Fig. S16, ESI†). The unit cell parameters, collected using single crystal XRD (SCXRD), revealed the decomposition products to be anthracene[32] and 9,10-anthraquinone.[33] In a separate experiment, PXRD patterns were also recorded on cooling the pristine sample to −153 °C (Fig. S14, ESI†). Apart from the expected subtle shift in peak positions due to the variable temperature, the peaks remained unaltered validating the stability of this material over a wide temperature window (Fig. S14 and S15, ESI†).

The electrochemical properties of $Na_2ADC(MW)$ were tested on electrodes prepared using a water-soluble binder, sodium alginate (details in experimental section). A first cycle discharge capacity of 266 mAh g^{-1} was achieved for an electrode containing 60 wt% active material cycled at a rate of 25 mA g^{-1} (Fig. S17, ESI†). The voltage profile indicated a two-step insertion process with plateaus for reduction at 0.69 and 0.55 V, and desodiation at 0.80 and 0.90 V (Fig. S17, ESI†). The stepwise insertion can be ascribed to involvement of the π-electrons in the first step before reaction with the carboxylate group, as previously noted for organic electrodes with a highly conjugated core.[34] The specific capacity stabilised at 100 mAh g^{-1} in the following cycles, with moderately stable performance over 50 cycles (Fig. S17 and S18, ESI†). The irreversible capacity in the first cycle could be ascribed to the formation of the solid–electrolyte interphase (SEI) and insertion of Na-ions into the conductive carbon (Fig. S19, ESI†).[35] To understand the stability of the material, an *ex situ* PXRD pattern was recorded upon sodiation, which showed retention of long-range order (Fig. S20, ESI†). The observed capacities were considerably lower than those for related sodium carboxylates. To understand the electrochemical properties further, the amount of conductive carbon was increased in steps of 10 wt%. Upon cycling electrodes containing 50 wt% active material, the redox peaks corresponding to Na-ion insertion were sharper, along with a noticeable reduction in the polarisation (Fig. S21, ESI†). This also resulted in improved specific capacities (Fig. S22 and S23a, ESI†). The performance was further enhanced for electrodes consisting of 40 wt% active material, with stable capacities of 200 mAh g^{-1} over 100 cycles (Fig. 3a). The considerable capacity improvement in electrodes having 40–50 wt% $Na_2ADC(MW)$ suggests the need for more conducting carbon to realise the potential of $Na_2ADC(MW)$ for charge storage. Although increasing loadings of conductive carbon has issues linked to lower volumetric densities, greater insertion of Na ions by the conductive carbon, and poorer initial coulombic efficiencies (ICE) (Fig. S24, ESI†), using 40 wt% $Na_2ADC(MW)$ gave good rate performance up to 1 A g^{-1} (Fig. 3b).

Despite differences in capacities, the specific capacities could be recovered for all compositions when the current density was reduced to 25 mA g^{-1} after step wise increases up to 1 A g^{-1} (Fig. S25, ESI†). The achieved capacities and ICE

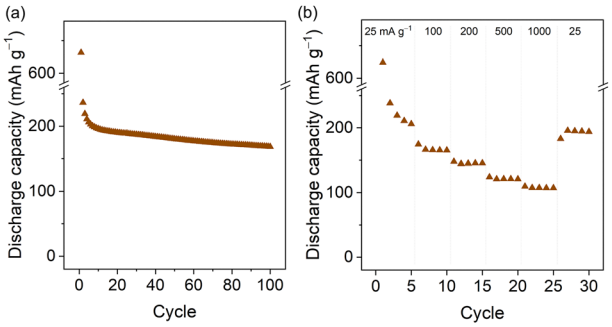

Fig. 3 (a) Discharge capacities over 100 cycles for $Na_2ADC(MW)$ [40 : 50 : 10, referring to the wt% ratio of active material : conductive carbon : binder], cycled at 25 mA g^{-1} between 0.01–2.5 V at 30 °C. (b) Rate performance, cycled five times at each current density.

values (Table S5, ESI†) for $Na_2ADC(MW)$ are lower than related sodium carboxylates, especially for higher loadings of the active material.[11] It is worth highlighting the differences in the structure, which may be responsible for this variation. It has been suggested in previous examples of similar OEMs that the inorganic (Na–O) sheets facilitate ion diffusion.[36] The absence of a sheet-like structure in $Na_2ADC(MW)$ and the presence of inorganic moieties well separated by dense organic components can be considered the cause of the greater barrier for ion diffusion. Although the extension of conjugation in the building unit, from benzene to anthracene, is typically expected to enhance the electronic conductivity, the lack of conjugation in the long-range structures has been shown to reduce this benefit.[37] In the case of $Na_2ADC(MW)$, the anthracene moieties are considerably more separated than the optimal interlayer distance for Na-ion insertion in sheets of sp^2 carbons (Fig. S26a, ESI†), as seen for hard carbon anodes.[38] Furthermore, the anthracene rings in $Na_2ADC(MW)$ are arranged in a parallel offset manner,[39] and the presence of multiple CH/π interactions for the same molecule may obstruct smooth ion diffusion (Fig. S26b and c, ESI†). This can be underscored by the improved performance of $Na_2ADC(MW)$ with higher amounts of conducting carbon.

In summary, disodium anthracene-9,10-dicarboxylate was synthesised using the greener method of microwave-assisted heating and investigated as an electrode material for sodium-ion batteries. Detailed material characterisation was carried out, including the determination of the crystal structure using electron diffraction. The material can reversibly insert sodium-ions, and optimised compositions delivered stable specific capacities in excess of 200 mAh g^{-1}. This work highlights the need to fully understand structure characteristics, and in this pursuit the effective use of 3D ED offers a new frontier for battery materials, especially OEMs, to have a better handle on structure–property correlation.

A. V. D., R. E. M. and A. R. A. thank the Faraday Institution for funding (grants – FIRG018, FIRG064). The authors also acknowledge the support from EPSRC for the Light Element Facility Grant (EP/T019298/1), Strategic Equipment Resource Grant (EP/R023751/1), and EPSRC Core Equipment Grant (EP/

V034138/1). H. S. S. thanks the Allan Handsel Postgraduate Research Scholarship for Chemistry for funding. D. N. R. and S. J. C. thank the EPSRC (EP/X014444/1) for funding.

Conflicts of interest

There are no conflicts to declare.

Data availability

The research data underpinning this article, including powder diffraction data, electrochemical test results, IR, Raman and NMR spectra can be accessed at **https://doi.org/10.17630/769658ed-3f8a-4175-8673-5991362c3b66**. The 3D ED raw data can be accessed at **https://doi.org/10.5281/zenodo.15705929**.

Notes and references

1 J. Y. Hwang, S. T. Myung and Y. K. Sun, *Chem. Soc. Rev.*, 2017, **46**, 3529–3614.
2 A. Rudola, R. Sayers, C. J. Wright and J. Barker, *Nat. Energy*, 2023, **8**, 215–218.
3 C. Vaalma, D. Buchholz, M. Weil and S. Passerini, *Nat. Rev. Mater.*, 2018, **3**, 18013.
4 P. K. Nayak, L. Yang, W. Brehm and P. Adelhelm, *Angew. Chem., Int. Ed.*, 2018, **57**, 102–120.
5 P. Poizot, J. Gaubicher, S. Renault, L. Dubois, Y. Liang and Y. Yao, *Chem. Rev.*, 2020, **120**, 6490–6557.
6 J. Kim, Y. Kim, J. Yoo, G. Kwon, Y. Ko and K. Kang, *Nat. Rev. Mater.*, 2023, **8**, 54–70.
7 H. Zhang, Y. Gao, X.-H. Liu, Z. Yang, X.-X. He, L. Li, Y. Qiao, W.-H. Chen, R.-H. Zeng, Y. Wang and S.-L. Chou, *Adv. Funct. Mater.*, 2022, **32**, 2107718.
8 T. Chen, J. Wang, B. Tan, K. J. Zhang, H. Banda, Y. Zhang, D.-H. Kim and M. Dincă, *J. Am. Chem. Soc.*, 2025, **147**, 6181–6192.
9 Y. Lu, Q. Zhang, L. Li, Z. Niu and J. Chen, *Chem*, 2018, **4**, 2786–2813.
10 R. Rajagopalan, Y. Tang, C. Jia, X. Ji and H. Wang, *Energy Environ. Sci.*, 2020, **13**, 1568–1592.
11 K. Holguin, M. Mohammadiroudbari, K. Qin and C. Luo, *J. Mater. Chem. A*, 2021, **9**, 19083–19115.
12 C. Puscalau, A. V. Desai, E. Lizundia, R. Ettlinger, M. Adam, R. E. Morris, A. R. Armstrong, B. Tokay and A. Laybourn, *Green Chem.*, 2025, **27**, 2035–2045.
13 M. Armand, S. Grugeon, H. Vezin, S. Laruelle, P. Ribière, P. Poizot and J.-M. Tarascon, *Nat. Mater.*, 2009, **8**, 120–125.
14 K. Qin, K. Holguin, M. Mohammadiroudbari and C. Luo, *Chem. Commun.*, 2021, **57**, 2360–2363.
15 J. Huang, K. I. E. Callender, K. Qin, M. Girgis, M. Paige, Z. Yang, A. Z. Clayborne and C. Luo, *ACS Appl. Mater. Interfaces*, 2022, **14**, 40784–40792.
16 D. M. Harrison, B. Bashir, E. Arkfeld, A. Z. Clayborne and C. Luo, *ACS Appl. Energy Mater.*, 2024, **7**, 4233–4242.
17 S. Lee, J. E. Kwon, J. Hong, S. Y. Park and K. Kang, *J. Mater. Chem. A*, 2019, **7**, 11438–11443.
18 K. Holguin, K. Qin, E. P. Kamphaus, F. Chen, L. Cheng, G.-L. Xu, K. Amine and C. Luo, *J. Power Sources*, 2022, **533**, 231383.
19 X. Yin, S. Sarkar, S. Shi, Q.-A. Huang, H. Zhao, L. Yan, Y. Zhao and J. Zhang, *Adv. Funct. Mater.*, 2020, **30**, 1908445.
20 Y. Qi, H. Zhao and Y. Lei, *Chem. Commun.*, 2025, **61**, 2375–2386.
21 I. Thomas-Hillman, L. A. Stevens, M. Lange, J. Möllmer, W. Lewis, C. Dodds, S. W. Kingman and A. Laybourn, *Green Chem.*, 2019, **21**, 5039–5045.
22 A. V. Desai, D. N. Rainer, A. Pramanik, J. M. Cabañero Jr., R. E. Morris and A. R. Armstrong, *Small Methods*, 2021, **5**, 2101016.
23 Z. Huang, T. Willhammar and X. Zou, *Chem. Sci.*, 2021, **12**, 1206–1219.
24 Z. Huang, E. S. Grape, J. Li, A. K. Inge and X. Zou, *Coord. Chem. Rev.*, 2021, **427**, 213583.
25 M. Nishio, *Phys. Chem. Chem. Phys.*, 2011, **13**, 13873–13900.
26 J. A. Kaduk, *Acta Crystallogr., Sect. B: Struct. Sci.*, 2000, **56**, 474–485.
27 Z. Cheng, H. Shi, H. Ma, L. Bian, Q. Wu, L. Gu, S. Cai, X. Wang, W. Xiong, Z. An and W. Huang, *Angew. Chem., Int. Ed.*, 2018, **57**, 678–682.
28 A. Choi, Y. K. Kim, T. K. Kim, M. S. Kwon, K. T. Lee and H. R. Moon, *J. Mater. Chem. A*, 2014, **2**, 14986–14993.
29 S. E. Ashbrook and M. J. Duer, *Concepts Magn. Reson., Part A*, 2006, **28A**, 183–248.
30 T. Whewell, V. R. Seymour, K. Griffiths, N. R. Halcovitch, A. V. Desai, R. E. Morris, A. R. Armstrong and J. M. Griffin, *Magn. Reson. Chem.*, 2022, **60**, 489–503.
31 J. M. Cabañero, V. Pimenta, K. C. Cannon, R. E. Morris and A. R. Armstrong, *ChemSusChem*, 2019, **12**, 4522–4528.
32 R. Mason, *Acta Crystallogr.*, 1964, **17**, 547–555.
33 K. Lonsdale, J. Milledge and K. El Sayed, *Acta Crystallogr.*, 1966, **20**, 1–13.
34 Y. Liu, X. Zhao, C. Fang, Z. Ye, Y.-B. He, D. Lei, J. Yang, Y. Zhang, Y. Li, Q. Liu, Y. Huang, R. Zeng, L. Kang, J. Liu and Y.-H. Huang, *Chem*, 2018, **4**, 2463–2478.
35 C. Bommier and X. Ji, *Small*, 2018, **14**, 1703576.
36 X. Wu, S. Jin, Z. Zhang, L. Jiang, L. Mu, Y.-S. Hu, H. Li, X. Chen, M. Armand, L. Chen and X. Huang, *Sci. Adv.*, 2015, **1**, e1500330.
37 A. M. Fraind and J. D. Tovar, *J. Phys. Chem. B*, 2010, **114**, 3104–3116.
38 C. Matei Ghimbeu, J. Górka, V. Simone, L. Simonin, S. Martinet and C. Vix-Guterl, *Nano Energy*, 2018, **44**, 327–335.
39 C. R. Martinez and B. L. Iverson, *Chem. Sci.*, 2012, **3**, 2191–2201.